We are IntechOpen,
the world's leading publisher of
Open Access books
Built by scientists, for scientists

6,000
Open access books available

148,000
International authors and editors

185M
Downloads

Our authors are among the

154
Countries delivered to

TOP 1%
most cited scientists

12.2%
Contributors from top 500 universities

CLARIVATE ANALYTICS
BOOK CITATION INDEX
INDEXED

WEB OF SCIENCE™

Selection of our books indexed in the Book Citation Index
in Web of Science™ Core Collection (BKCI)

Interested in publishing with us?
Contact book.department@intechopen.com

Chapter

Chiral Ice Crystals in Space

Akira Kouchi, Takashi Shimonishi, Tomoya Yamazaki,
Masashi Tsuge, Naoki Nakatani, Kenji Furuya,
Hiromasa Niinomi, Yasuhiro Oba, Tetsuya Hama,
Hiroyasu Katsuno, Naoki Watanabe and Yuki Kimura

Abstract

We observed the formation of CO, CH_3OH, and H_2O ices using a cryogenic transmission electron microscope, to determine if chiral ice crystals could form under the conditions of interstellar molecular clouds and young stellar objects (protoplanetary disks) and to clarify the crystalline structure of these ices. Our results suggest that the following ice crystals are chiral: crystalline CO (α-CO) formed on amorphous H_2O (a-H_2O) grains in a 10-K molecular cloud, crystalline CH_3OH formed by the heating of amorphous CH_3OH on a-H_2O grains at 40–60 K in young stellar objects, and several polymorphs of hydrogen-ordered cubic ice crystals formed by the heating of a-H_2O at 80–100 K and direct condensation at 120–140 K in protoplanetary disks. We also investigated candidates for other chiral ices using published data. We found that NH_3 I and $NH_3 \cdot H_2O$ I are chiral at low temperature and pressure conditions. If one-handed circularly polarized light is irradiated during the nucleation of these chiral ice crystals, homochiral crystals can be formed. These results have important implications for the origin of interstellar organic molecule homochirality.

Keywords: ice crystals, chirality, CO, H_2O, CH_3OH, NH_3, interstellar molecular cloud, protoplanetary disk, circularly polarized light, asymmetric nucleation

1. Introduction

The origin of biomolecular homochirality is one of the most important mysteries of the origin of life. However, asymmetric adsorption and/or asymmetric synthesis on inorganic crystal surfaces is a possible candidate for chiral selection [1–3]. Quartz and cinnabar are regarded as chiral crystals, and it has been suggested that the surfaces of achiral crystals (e.g., gypsum, calcite, and alkali feldspar) can act as chiral faces [2, 4]. These minerals, as both chiral and achiral crystals, could be formed in evolved bodies, such as meteoritic parent bodies and terrestrial planets; however, it is implicitly considered that there were/are no chiral crystals in interstellar grains. Using transmission electron microscopy (TEM), we demonstrated that chiral crystalline CO (α-CO) would form on icy grains in interstellar molecular clouds [5]; therefore, α-CO in molecular clouds could be regarded as the first chiral crystal in space. To build on this finding, we searched for other chiral ices in space via further laboratory

experiments and literature searches. We used the term "ice" to describe a solid at low temperatures (e.g., H_2O, CO_2, CO, NH_3, CH_3OH, and their hydrates).

In this chapter, after a brief explanation of icy grains in space in Section 2, we describe the crystal structures of each chiral ice in Section 3. In Section 4, a formation mechanism for homochiral ice crystals in space is discussed. In Section 5, we suggest further areas of study for the determination of the origin of the homochirality of organic molecules on icy grains in space.

2. Icy grains in space

2.1 The evolution of icy grains during the formation of the solar system

The evolution of icy grains, from an interstellar molecular cloud to a solar system, is schematically illustrated in **Figure 1**. In 10-K interstellar molecular cloud, icy grains were composed of an amorphous silicate (a-silicate) core, an inner organic mantle, an outer icy mantle of amorphous H_2O (a-H_2O), and α-CO attached to a-H_2O mantle [6]. The composition of ice differs among molecular clouds, as shown in **Table 1**. The molecular cloud collapsed by gravitational contraction to form protosolar nebulas, during which the icy grains were heated according to their heliocentric distance. In the inner region, the grains were completely sublimated. However, in the outer region, some grains survived. Subsequent cooling led to the formation of crystalline silicates in the inner region and H_2O ice crystals in the Jovian region. The aggregation of these
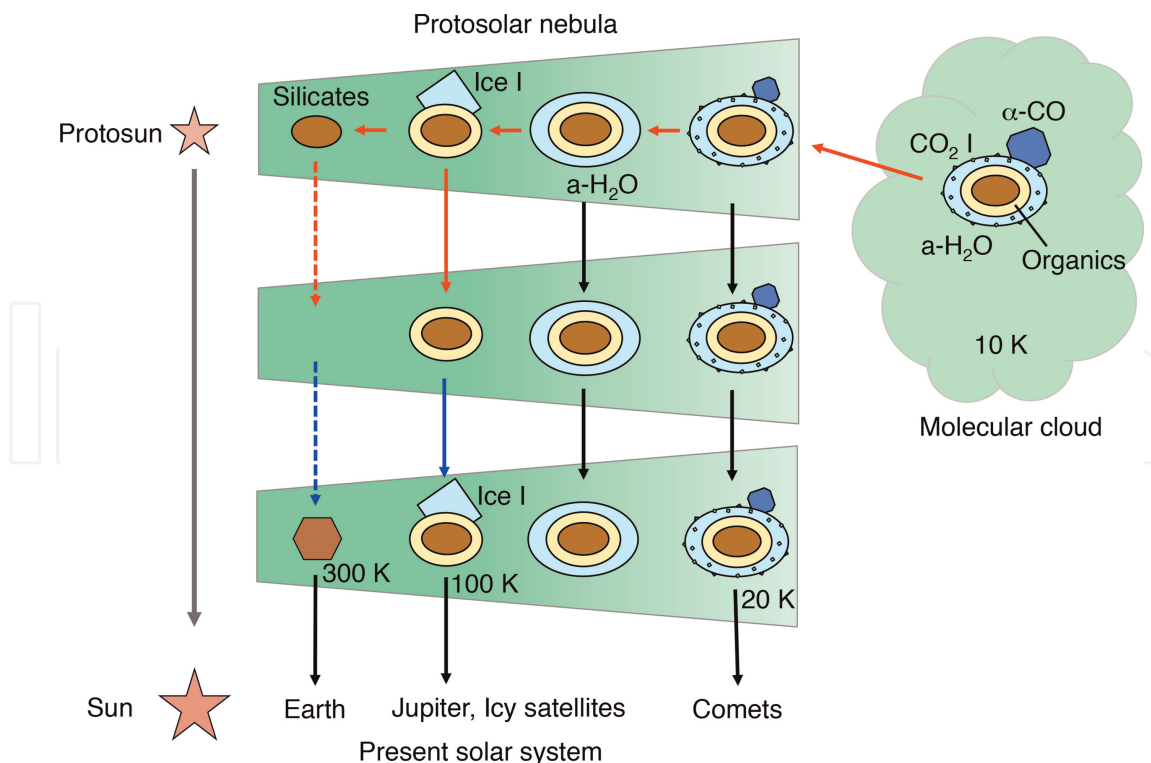

Figure 1.
Evolution of icy grains in space (grain sizes < 1μm). The compositions of the grains are indicated by different colors: Blue: CO, pale blue: H_2O, yellow: Organic matter, and brown: Silicate. Note that CH_3OH, NH_3, and minor components have been omitted for simplicity. Oval and polygonal grain forms are amorphous and crystalline, respectively. The density of the nebular gas, mainly composed of H_2, is indicated by the intensity of the green filling. The red and blue arrows indicate heating and cooling, respectively.

Molecule	MCs	MYSOs	LYSOs	Comets
H_2O	100	100	100	100
CO	9–67	3–26	(<3)–85	0.4–30
CO_2	14–43	11–27	12–50	4–30
CH_3OH	(<1)–12	(<3)–31	(<1)–25	0.2–7
NH_3	<7	~7	3–10	0.2–1.4
CH_4	<3	1–3	1–11	0.4–1.6
H_2CO	n.d.	2–7	~6	0.11–1
HCOOH	<2	(<0.5)–6	(<0.5)–4	0.06–0.14
NH_4^+	4–13	9–34	4–25	n.d.

Table 1.
Composition of ice in molecular clouds [7], young stellar objects [7], and comets [8] relative to H_2O. Abbreviations: MC, molecular cloud; MYSO, massive young stellar object; LYSO, low-mass young stellar object; n. d., no data.

grains led to the formation of planets via planetesimals, and remnant planetesimals from this outer region are the comets we observe today.

2.2 Infrared observation of ices

Information about the composition and crystallinity of icy grains can be gained from infrared (IR) astronomical observations. **Table 1** lists the main components of icy grains observed in molecular clouds and young stellar objects [7], including comets [8]. The most abundant component for all the objects is H_2O. The next most abundant components are CO and CO_2, although the abundance of CO varies depending on the object. For all the objects, the abundance of CH_3OH relative to H_2O ranges from lower than the detection limit to ~30%. Because CH_3OH can be formed from CO via the H-atom addition reaction on icy grains [9], it is suggested that the amount of CH_3OH reflects the evolutionary stage of objects. Although NH_3 is not detected in molecular clouds, it is detected in young stellar objects, while considerable amounts of NH_4^+ are tentatively assigned to all the objects [7]. It should be noted that the composition of cometary ices is quantitatively consistent with that of interstellar ices, suggesting an interstellar origin for cometary ices [8]. Among the crystals of these abundant molecules, possible chiral crystal candidates are H_2O, CO, CH_3OH, NH_3, and their hydrates, which will be discussed in the following section.

The comparison of astronomically observed and laboratory-measured IR spectra provides us with information on the crystallinity of ices, both amorphous and crystalline. H_2O ice is easily identified because of the spectral feature of the OH stretching mode around 3 μm, which differs between amorphous and crystalline H_2O ices [10]. The observed features of a molecular cloud (Elias 16) and a circumstellar envelope of an evolved star (OH231.8 + 4.2) could be fitted by a-H_2O at 23 K and crystalline H_2O ice at 77 K, respectively [11]. For a young stellar object (Orion BN), the observed feature could be fitted by a mixture of a-H_2O at 23 and 77 K and crystalline H_2O ice at 150 K [11]. These results, consistent with a theoretical study [12], are reflected in the crystallinity of the H_2O ice depicted in **Figure 1**.
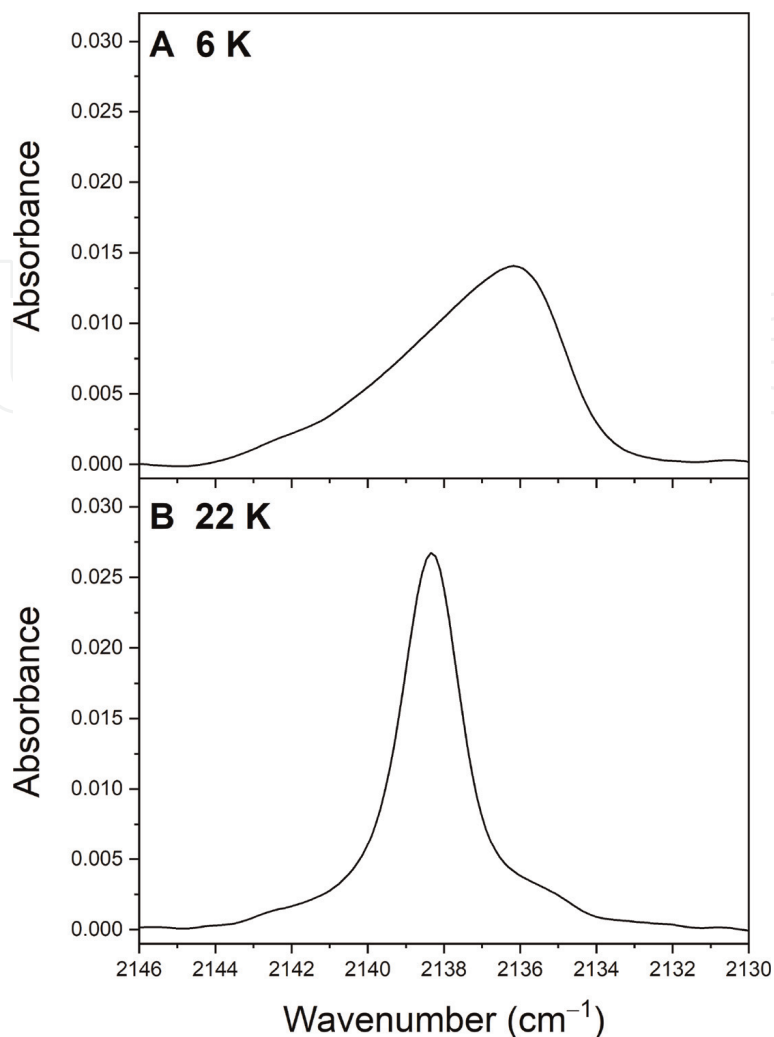
Figure 2.
Infrared spectra of solid CO. The CO gas was vapor deposited onto a Si(111) substrate at 6 K. The pressure of the chamber during deposition was 7.1×10^{-6} Pa (base pressure $< 2 \times 10^{-7}$ Pa), corresponding to the flux of 2×10^{13} molecules cm^{-2} s^{-1}, and the deposited amount after 60 minutes deposition was estimated to be 1.5×10^{17} molecules cm^{-2}. The deposited sample was warmed up stepwise with an increment of 2 K. The IR spectra were measured with a transmission configuration. The spectra measured at 6 K (a-CO) and 22 K (α-CO) are shown in (A) and (B), respectively.

Figure 2 shows the IR spectra of a-CO and α-CO measured by us. The sample deposition was done at a very low temperature (6 K) with a slow deposition rate (2×10^{13} molecules cm^{-2} s^{-1}), ensuring that the produced CO ice sample is amorphous [5]. The IR spectrum measured just after deposition shows an asymmetric feature with a peak near 2136 cm^{-1}: the IR spectrum of a-CO. During warming up to 22 K, the band shape gradually changed. The IR spectrum measured at 22 K (**Figure 2B**) shows a rather symmetric feature with a peak near 2138 cm^{-1}: the IR spectrum of α-CO. Recently, He et al. [13] reported the IR spectra of solid CO measured with a reflection-absorption IR spectrometry. They observed a very slight change in the peak position ($\sim$1 cm^{-1}) during warm-up and attributed this change to the phase transition from a-CO to α-CO. However, it should be noted that determination of crystallinity based on a reflection-absorption IR spectrometry measurement tends to be difficult and it is probable that their ice sample after deposition could be a mixture of a-CO and α-CO. Thus, we consider that the spectra shown in **Figure 2** are the first IR spectra of "pure" a-CO and α-CO measured in a laboratory. It is expected

Species	Phase	Space group	H-order	T (K)	Method [Ref]
H_2O	XIh[a]	$P2_1$	O		T [28]
	XIh[b]	$P2_12_12_1$	O		T [28]
	XIc[c]	$P2_1$	O		T [28]
	XIc[d]	$P2_12_12$	O		T [28]
	XIc[e]	$P4_12_12$	O		T [28]
	XIc[f]	$P4_1$	O		T [29]
	III[g]	$P4_12_12$	D	250	N [31]
CO	α	$P2_13$	n/a	14–30	N [19], E [5]
CH_3OH	α	$P2_12_12_1$	O	15, 110	N [33], E [34]
NH_3	I	$P2_13$	O	77	X [37], N [38]
$NH_3 \cdot H_2O$	I	$P2_12_12_1$	O	~110	X [37], N [42]
$NH_3 \cdot 2H_2O$	I[h]	$P2_12_12_1$	O	100	X [17]
		$P2_13$	PO	4–174	N [42, 44]
CH_4	II[h]	$P2_13$	O	12, 25	I [46]
		$P2_13$	O		T [47]
		$Fm\overline{3}c$	PO	24.5	N [48]

[a]*Hydrogen-ordered hexagonal ices called H12–H15 by Raza et al. [28].*
[b]*Hydrogen-ordered hexagonal ices called H6 and H7 by Raza et al. [28].*
[c]*Hydrogen-ordered cubic ices called C10 and C11 by Raza et al. [28].*
[d]*Hydrogen-ordered cubic ice called C7 by Raza et al. [28].*
[e]*Hydrogen-ordered cubic ice called C2 by Raza et al. [28].*
[f]*Hydrogen-ordered cubic ices called d by Geiger et al. [28].*
[g]*High-pressure ice, measured at 0.28 GPa.*
[h]*Two space groups have been proposed.*

Table 2.
Candidate chiral ice crystals in molecular clouds and protoplanetary disks. Abbreviations: O, order; D, disorder; PO, partial order; T, theory; N, neutron diffraction; X, X-ray diffraction; E, electron diffraction; I, far-infrared spectroscopy.

that a comparison of these laboratory spectra with astronomical observations will be made in the near future, which will further the discussion of the crystallinity of solid CO in molecular clouds.

The laboratory-measured spectra of amorphous and crystalline CH_3OH phases differ [14]; however, because the astronomically observed spectra of the OH stretching modes of CH_3OH overlap with those of H_2O, it is difficult to obtain information about the crystallinity of CH_3OH. Zanchet et al. [15] measured the near- and mid-IR spectra of amorphous and crystalline NH_3 at 15 and 85 K, respectively, and found that both spectra were similar, except for a band around 1100 cm^{-1} [15], which demonstrates the difficulty of obtaining information on the crystallinity of NH_3. At 83 K, the measured IR spectra of the amorphous and crystalline phases of $NH_3 \cdot H_2O$ differ between 700 and 1100 cm^{-1} [16], and only a crystalline phase has been measured for $NH_3 \cdot 2H_2O$ at 100 K [17]. However, it is expected that a comparison of these laboratory spectra with astronomical observations will be made in the near future.

3. The crystal structures of ices at low temperatures and pressures

Table 2 lists chiral ice crystal candidates in molecular clouds and protoplanetary disks, and the crystal structures of the respective species are described based on our observations and published data.

3.1 CO

α-CO is a thermodynamically stable phase of solid CO at low temperatures [18]. We observed the morphology of CO deposited on a-H_2O by TEM, as shown in **Figure 3** [5]. The CO formed three-dimensional polyhedral crystals, and the diffraction pattern confirmed that the CO crystals were α-CO. It has long been debated whether the crystal structure of α-CO is an orientationally ordered phase (space group: $P2_13$) or a disordered one (space group: $Pa\overline{3}$). Wang et al. [19] confirmed by neutron diffraction that α-CO belongs to $P2_13$, as proposed by Vegard [20]. Therefore, we concluded that α-CO in molecular clouds would be chiral.

3.2 H_2O

3.2.1 Ice Ih, Ic, and XI

Hydrogen-disordered hexagonal ice (ice Ih) is a thermodynamically stable phase of solid H_2O under low pressures at temperatures >72 K [21]. At temperatures <72 K, hydrogen-ordered ice XI becomes the thermodynamically stable phase [22, 23]. It is widely accepted that doping (e.g., KOH) is essential for the formation of ice XI at low temperatures [24]. A thermodynamically metastable phase of hydrogen-disordered cubic ice (ice Ic) also exists at temperatures between 100 and 200 K [21]. The crystal structures of ice Ih and ice Ic are very similar except for the stacking sequences of their layers: ice Ih is ABABAB and ice Ic is ABCABC. The space groups of ice Ih, ice XI,
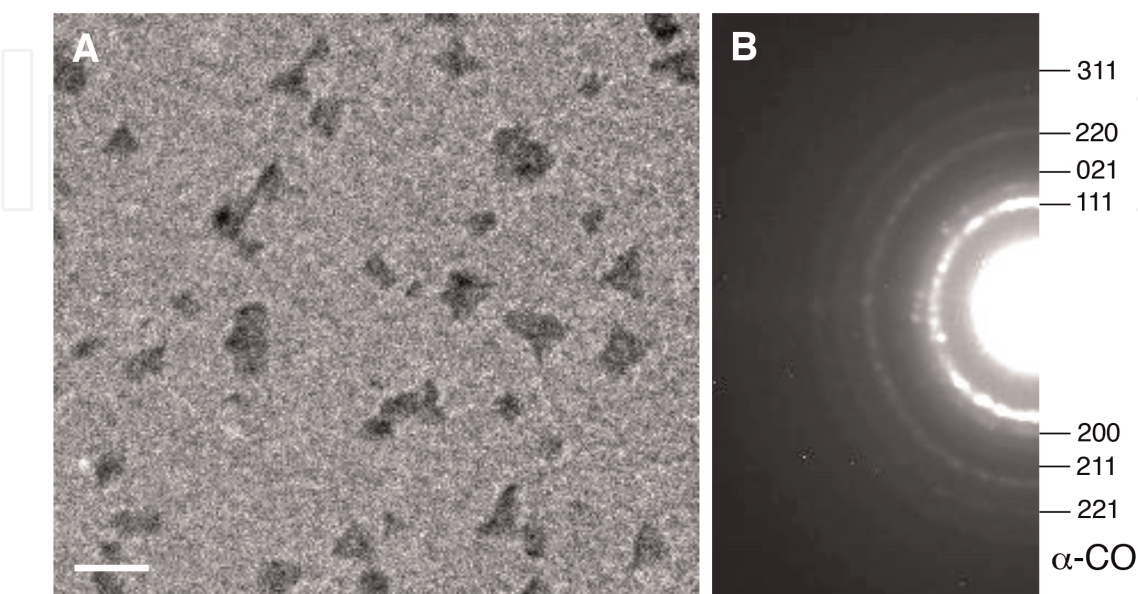
Figure 3.
Transmission electron microscopy image of (A) crystalline CO (α-CO) deposited on amorphous H_2O at 19 K, and (B) the electron diffraction pattern of α-CO on amorphous Si at 19 K. White scale bar = 500 nm.

and ice Ic are $P6_3/mmc$, $Cmc2_1$, and $F\bar{d}3m$, respectively, and all these crystals are not chiral.

3.2.2 Hydrogen-ordered cubic ice

Although the existence of hydrogen-ordered cubic ice (ice XIc) has been discussed theoretically [25–29], there has been no experimental evidence for this crystal structure. Raza et al. [28] and Geiger et al. [29] suggested 11 and 4 different structures, respectively, for ice XIc. We observed the annealing of ice Ic deposited on an a-SiN thin film by TEM and found that several polymorphs of ice were formed at temperatures between 100 and 130 K without doping [30]. **Figure 4** represents the TEM images and corresponding electron diffraction patterns of the ice XIc formed by the annealing of a-H_2O and ice Ic, showing the formation of ice XIc. However, we could not determine which structures were formed in terms of the different structures
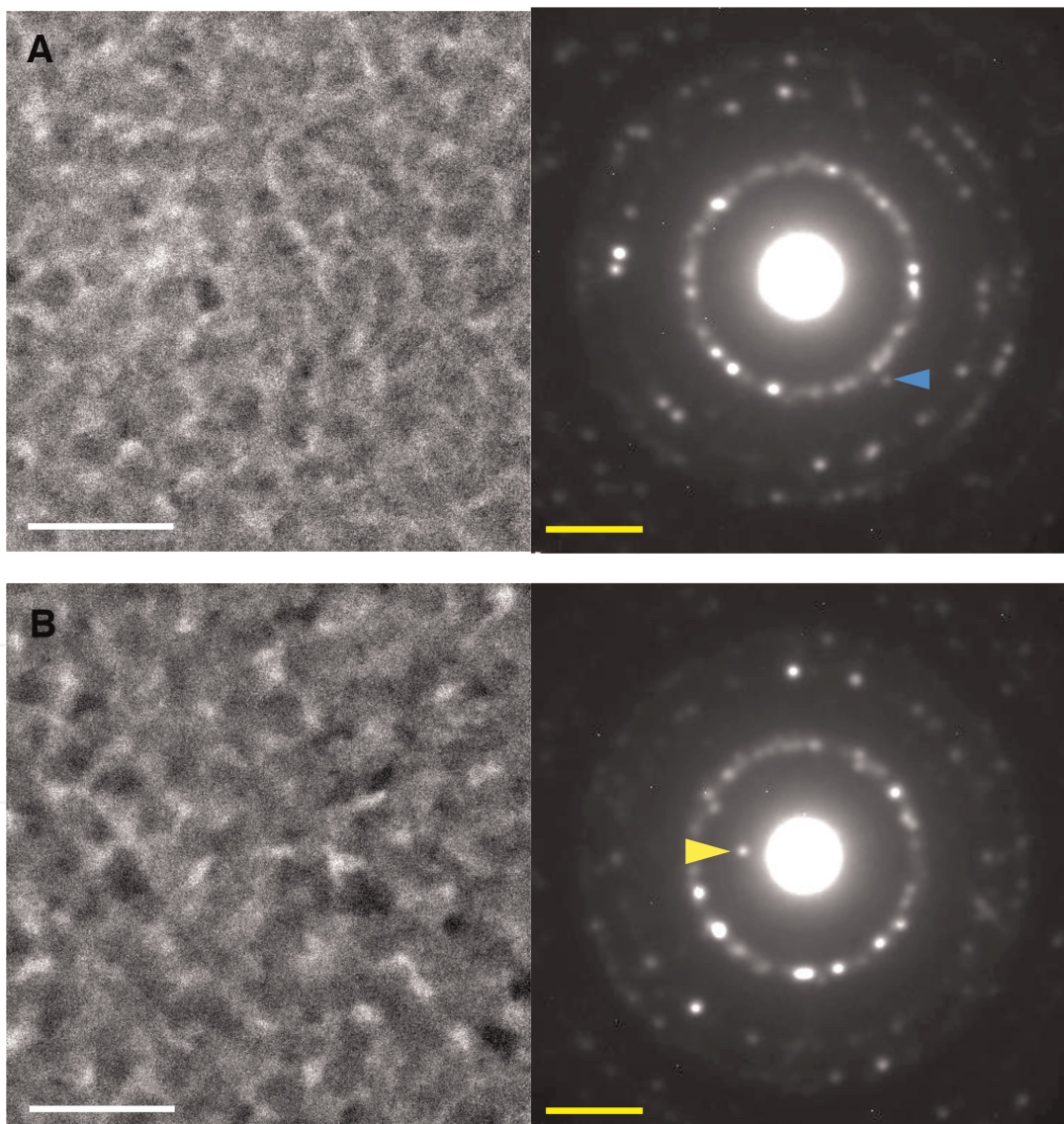

Figure 4.
Transmission electron microscopy images and corresponding electron diffraction patterns of hydrogen-ordered cubic ice (ice XIc) formed by (A) the annealing of amorphous H_2O at 130 K and (B) the annealing of ice Ic at 130 K. The blue and yellow arrowheads indicate the diffraction spots of $d = 4.50$ Å and $d = 6.41$ Å, respectively, originating from ice XIc. The white and yellow scale bars are 500 nm and 2 nm^{-1}, respectively.

proposed by Raza et al. [28] and Geiger et al. [29]. However, because five-twelfths of the proposed structures were chiral (space group: $P4_12_12$, $P2_12_12$, $P2_1$, and $P4_1$), some chiral crystals might be included not only in our samples but also in H_2O ice crystals in space. Furthermore, the calculation of the infrared spectra of ice XIc, as demonstrated by Geiger et al. [29], will help identify ice XIc in space.

3.2.3 Hydrogen-ordered hexagonal ice

As mentioned in Section 3.2.1, the thermodynamically stable phase of hydrogen-ordered hexagonal ice is ice XI. However, Raza et al. [28] proposed 15 different structures of hydrogen-ordered hexagonal ice (XIh) as metastable phases, and seven-fifteenths of the proposed structures are chiral (space group: $P2_12_12_1$, $P2_1$, and $P1$). Although there has been no experimental investigation of this, we should consider the occurrence of these polymorphs, as demonstrated in the Section 3.2.2.

3.2.4 Ice III

Here, it is worthwhile commenting on the structure of ice III, although ice III is stable only at higher pressures between 210 and 344 MPa and higher temperatures between 238 and 256 K [21]. The space group of ice III is $P4_12_12$, meaning that the arrangement of the oxygen atoms is ordered and chiral. Conversely, the arrangement of the hydrogen atoms is disordered [31]. Therefore, we concluded that the surface of ice III does not behave as an asymmetric catalyst on which asymmetric adsorption and/or asymmetric synthesis can proceed.

3.3 CH_3OH

α-CH_3OH is a thermodynamically stable phase of solid CH_3OH at temperatures < 157 K under low pressure [32]. Torrie et al. [33] showed by neutron diffraction that α-CH_3OH is chiral, including the positions of the hydrogen atoms (space group: $P2_12_12_1$). Furuya et al. [34] observed the deposition of CH_3OH on a-H_2O using TEM between 90 and 120 K and found that α-CH_3OH was formed at temperatures >100 K; however, they did not observe the crystallization of amorphous CH_3OH (a-CH_3OH). Using TEM, we observed the formation of α-CH_3OH crystals during the warming of a-CH_3OH deposited on a-H_2O (**Figure 5**). Therefore, we concluded that if α-CH_3OH crystals were formed by the heating of a-CH_3OH on a-H_2O grains in young stellar objects (i.e., protoplanetary disks), α-CH_3OH were/are chiral.

Sugisaki et al. [35] observed by calorimetry that the glass transition and crystallization of glassy CH_3OH occurred at about 103 and 105 K, respectively. Luna et al. [14] also observed by IR spectroscopy that the crystallization temperature of a-CH_3OH is between 100 and 110 K.

3.4 NH_3 and its hydrates

3.4.1 NH_3

NH_3 I is a thermodynamically stable phase of solid NH_3 at temperatures <200 K under low pressure [36]. Olovsson and Templeton [37] and Reed and Harris [38] showed by X-ray diffraction and neutron diffraction, respectively, that NH_3 I at 77 K is chiral, including the positions of the hydrogen atoms (space group: $P2_13$). Hewat
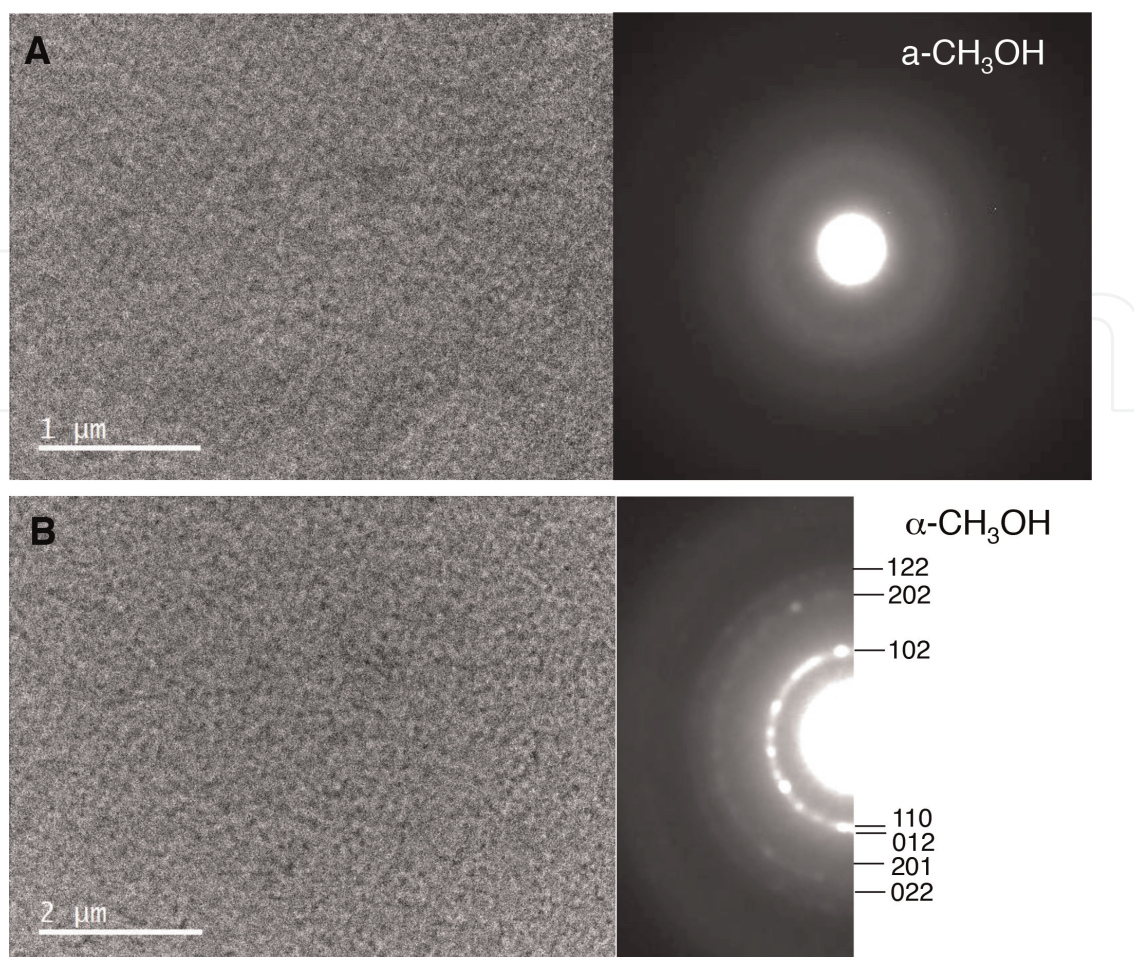
Figure 5.
Transmission electron microscopy image and corresponding electron diffraction pattern of (A) amorphous CH₃OH (a-CH₃OH) deposited on amorphous H₂O (a-H₂O) at 82 K and (B) those of crystalline CH₃OH (α-CH₃OH) at 110 K formed during the heating of a-CH₃OH.

and Riekel [39] also confirmed this by high-accuracy neutron diffraction at temperatures between 2 and 180 K. It has been observed by IR spectroscopy that the crystallization temperature of a-NH₃ is ∼80 K [39, 40].

3.4.2 $NH_3 \cdot H_2O$

$NH_3 \cdot H_2O$ I is a thermodynamically stable phase of solid $NH_3 \cdot H_2O$ at temperatures <194 K under low pressure [41]. Olovsson and Templeton [37] showed by X-ray diffraction that $NH_3 \cdot H_2O$ I at 113 K is chiral, including the positions of the hydrogen atoms (space group: $P2_12_12_1$). Loveday and Nelmes [42] confirmed the space group by neutron diffraction at 110 K.

3.4.3 $NH_3 \cdot 2H_2O$

$NH_3 \cdot 2H_2O$ I is a thermodynamically stable phase of solid $NH_3 \cdot 2H_2O$ at temperatures <176 K under low pressure [43]. Bertie and Shehata [17] showed by X-ray diffraction and IR spectroscopy that $NH_3 \cdot 2H_2O$ I at 100 K is chiral, including the positions of the hydrogen atoms (space group: $P2_12_12_1$). However, neutron diffraction studies showed that the space group is $P2_13$ and the hydrogen is partially ordered at

temperatures between 4 and 174 K [42, 44]. Among the four hydrogen sites, the hydrogen occupancy of two of the sites was unity (order), while those of the other two sites were one-third and two-thirds. They considered that the transition to the ordered phase is frustrated by kinetics, as in the transition of pure ice Ih to ice XI. Fortes et al. [44] suggested the occurrence of a hydrogen-ordered phase (space group: $P2_12_12_1$) at temperatures <140 K because the ordered phase must be thermodynamically more stable than the disordered phase at low temperatures. We therefore suggested the occurrence of a hydrogen-ordered phase (space group: $P2_12_12_1$) at lower temperatures in space, although the equilibrium structure at low temperatures still remains unclear. Further studies on the formation of the ordered phase using a dopant should be undertaken.

3.5 CH₄

CH$_4$ II is a thermodynamically stable phase of solid CH$_4$ at temperatures <20.4 K under low pressure [45]. Savoie and Fourier [46] suggested that the CH$_4$ II space group is $P2_13$ based on the measurement of far-IR spectra at 12 and 25 K. Hashimoto et al. [47] also suggested the same space group based on the calculation of pair-interaction potentials. Press [48] showed by neutron diffraction at 24.5 K that six of the eight molecules were ordered while the remaining two were orientationally disordered, with a space group of $F\text{m}\overline{3}\text{c}$. Kobashi et al. [49], based on IR and Raman spectra, suggested that, theoretically, the space group of CH$_4$ II is $F\text{m}\overline{3}\text{c}$. Greiger et al. [50] analyzed the total neutron cross section assuming the structure proposed by Press [48]. Although recent studies have only referred to $F\text{m}\overline{3}\text{c}$, these results do not rule out the existence of the space group $P2_13$. Therefore, we cannot eliminate the possibility that both space groups exist.

4. The formation of homochiral ice crystals

4.1 Sources of circularly polarized light

One-handed circularly polarized light (CPL) from an astronomical source could play an essential role in the homochirality of ice crystals. Neutron stars have been suggested as possible sources of CPL [51]; however, CPL at visible and UV wavelengths has not been observed [52], and it is unlikely that a neutron star could encounter a molecular cloud where our solar system was born [53]. In contrast, CPL produced in star-forming regions is considered to be more important because CPL has been observed [54], and the possibility of a star-forming region and a molecular cloud occurring together is very large. Therefore, our discussion of the homochirality of ice crystals assumes that the CPL originated in a star-forming region.

4.2 CPL flux in a molecular cloud

We estimated the CPL photon flux in a molecular cloud based on a simplified model. We assumed two cases: i) a molecular cloud illuminated by the interstellar radiation field and ii) a molecular cloud illuminated by radiation from a nearby massive star. Case i) assumed an isolated star formation, while case ii) assumed a clustered star formation in a massive star-forming region. In both cases, we assumed a

0.1 pc diameter molecular cloud with a hydrogen density of 2×10^5 cm^{-3}. We used Weingartner and Draine's [55] standard dust extinction curve with an R_V parameter of 5.5 to mimic dust in dense clouds [56].

For i), a standard interstellar radiation field model [57] was assumed for the incident radiation spectrum. For (ii), the incident radiation field was simulated by blackbody radiation from a B3-type star (mass = 8 solar mass, luminosity = 2.8×10^3 solar luminosity, and surface effective temperature = 2.3×10^4 K), which was located 0.1 pc away from the molecular cloud. IR observations have indicated that circularly polarized IR emissions with a degree of circular polarization of up to 20% extend in a 0.1–0.7 pc area in high−/intermediate-mass star-forming regions [58, 59].

We assumed that the CPL was generated within the molecular cloud by the dichroic extinction of incident radiation [60]. A theoretical study predicted that dichroic extinction can produce a degree of circular polarization of up ∼10% in star-forming clouds [61]. Here, we assumed that the radiation penetrating the molecular cloud resulted in a 10% degree of circular polarization.

The estimated flux of the CPL in the molecular cloud is summarized in **Figure 6**. On the surface of the molecular cloud, the photon flux reflects sources of radiation and does not change with wavelength. At the middle points (r = 0.025 pc), however, the photon flux decreases with decreasing wavelength. The intensities of the photon fluxes at 200 nm in the cases of i) and ii) were $\sim 10^{-1}$ and $\sim 10^3$ photons cm^{-2} s^{-1}, respectively, suggesting that the photon flux of case i) was too weak for a photo-chemical reaction but that of case ii) was effective.

We noted that cosmic-ray-induced UV (CRUV) is a dominant source of UV photons in well-shielded regions [62, 63]. The total photon flux of CRUV is estimated to
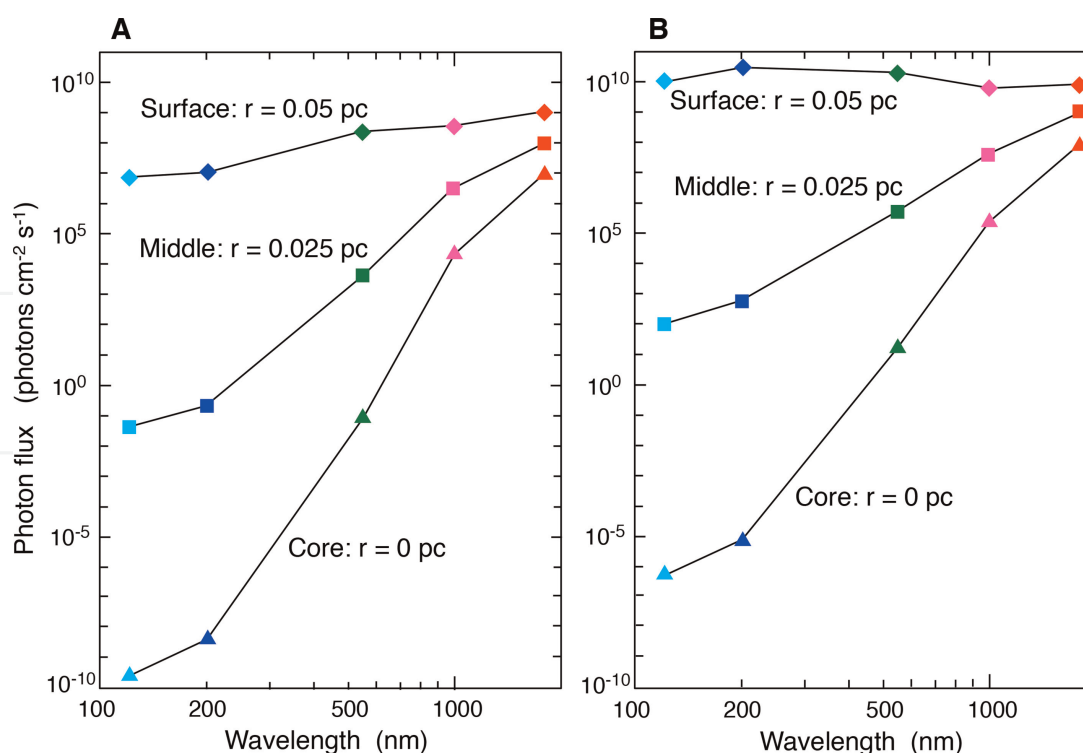

Figure 6.
The wavelength dependence of the flux of circularly polarized light in the molecular cloud. For incident radiation sources, (A) and (B) assume an interstellar radiation field and blackbody radiation from a massive star, respectively. The respective colored marks represent the photon fluxes integrated over the following wavelength regions: Cyan, 90–150 nm; blue, 150–250 nm; green, 400–700 nm; magenta, 800–1200 nm; and red, 1000–2600 nm.

be 10^4 photons cm^{-2} s^{-1} [64], which is orders of magnitude higher than the estimated photon fluxes at the middle and core points in cases i) and ii). However, because CRUV photons are produced in dense regions, they would be irradiated to icy grains before experiencing dichroic extinction. Thus, we did not consider CRUV to be a source of CPL. If circularly polarized UV light plays an important role in the production of enantiomeric excess, then relevant photo processing would occur on the shallow molecular cloud surface, where the external UV overwhelms the CRUV. Because the volume fraction of the middle part of the molecular cloud is ~0.88, we discuss the asymmetric nucleation of ice crystals using a curve at the middle points (r = 0.025 pc) in the following section.

4.3 Asymmetric nucleation by one-handed CPL

Solid CO is formed via CO deposition from the vapor phase in molecular clouds. The crystallinity of solid CO, either amorphous or crystalline, can be determined by the CO flux in a molecular cloud [5]. Because the CO flux in a molecular cloud is much smaller than the critical flux in which amorphous CO (a-CO) is formed, α-CO should be formed. When one-handed CPL is irradiated during the nucleation of α-CO, the formed crystals might have an enantiomeric excess (**Figure 7**). When there are no metal or high-index nanoparticles on icy grains, α-CO can absorb UV-CPL, which may result in excess enantiomeric crystals. In this case, the formation of one-handed α-CO would only occur in the shallow part of the molecular cloud because the UV-ray penetration depth is not so large (see **Figure 6**). However, when there are metal or high-index nanoparticles on the icy grains, the peak absorption wavelength could be transferred to the visible wavelength region, and the peak could be enhanced compared to that of the UV region [65–67], resulting in excess enantiomeric crystals, possibly up to several tens of percent. This could be supported by laboratory
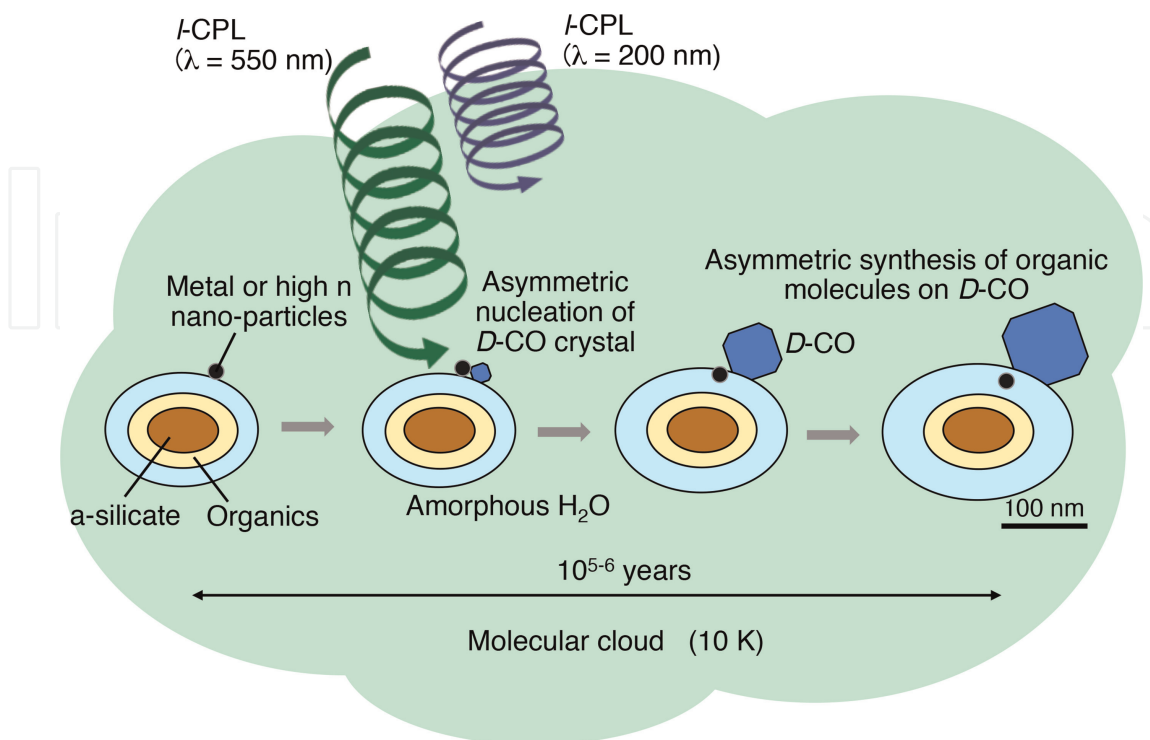
Figure 7.
Schematic illustration of the formation of homochiral CO crystals on the icy grains in molecular clouds.

experiments on chiral crystallization [68, 69] and theoretical work [70–72]. In this case, the formation of one-handed α-CO would occur not only in shallow parts of a molecular cloud but also in deeper parts because the penetration depth of visible rays is considerably deep (see **Figure 6**).

A similar process might occur during the crystallization of a-H_2O to form chiral ice crystals and hydrogen-ordered cubic and hexagonal ices (see **Table 2**) in protosolar nebula, as shown in **Figure 1**. The crystallization temperature of a-H_2O under a 10^5-years' timescale is ∼90 K [12]. The penetration depth of UV to visible CPL in protoplanetary disks is smaller than that in molecular clouds. However, icy grains could be moved to the surface of the disk by turbulent motion [73] and irradiated with CPL, resulting in the formation of one-handed, hydrogen-ordered H_2O crystals. When ice crystals were recondensed during the cooling of the solar nebula (**Figure 1**), one-handed, hydrogen-ordered H_2O crystals might be formed by the same mechanism.

The crystallization of a-CH_3OH and a-NH_3 also occurred in the protoplanetary disk. Crystallization temperatures of a-CH_3OH and a-NH_3 under a 10^5-years' time-scale can be estimated from those in the laboratory (a-CH_3OH: ∼100 K [14, 35] and a-NH_3: ∼80 K [15, 40]) and from the assumption that the slopes of a-CH_3OH and a-NH_3 in the plot of the timescale of crystallization vs. the inverse of the temperature lie between those of H_2O [12] and CO_2 [6]. We found that the crystallization temperatures of a-CH_3OH and a-NH_3 under the 10^5-years' timescale were 40–60 K and 20–40 K, respectively. The formation of one-handed α-CH_3OH, NH_3 I, and NH_3 hydrates might also occur, as in the crystallization of a-H_2O. In this way, various kinds of homochiral ice crystals could be formed in protoplanetary disks.

5. Conclusion and outlook

The results of this study indicate the possibility that there were/are many chiral ice crystals in space and that homochiral ice crystals might form by the irradiation of CPL in the star-forming region. These findings have important implications for the origin of the homochirality of organic molecules in space, and the pursuit of the following three suggested areas of study would further our understanding of this.

The crystallinity of CH_3OH and NH_3 in space and the formation mechanism of α-CH_3OH, NH_3 I, and their hydrates in protoplanetary disks are still unclear. Therefore, astronomical observations of the crystallinity of these ices are highly desirable.

For chemical reactions on icy grains, only a-H_2O ice has been considered as a substrate. The adsorption and subsequent surface diffusion of atoms (H, C, N, and O), small molecules (e.g., CO, CO_2, and H_2CO), and radicals (e.g., OH, HCO, and NH), followed by surface two-body reactions to form larger molecules on a-H_2O at low temperatures have been calculated using astrochemical reaction network models [74]. However, this study indicated the possibility of the growth of single ice crystals on grains. On the surface of α-CO, the adsorption behavior of atoms differs greatly from that on a-H_2O [6]. Therefore, it is expected that atoms, except for C and small molecules/radicals, are not adsorbed on the surface of singe-crystalline H_2O ice I. Instead, larger molecules/radicals diffuse easily on the surface of singe-crystalline H_2O ice I, which leads to the formation of more complex organic molecules. Furthermore, the asymmetric adsorption/synthesis of organic molecules on homochiral ice crystals might also proceed.

The search for enantiomeric surfaces on achiral ice crystals, as investigated in minerals [2, 4], is another important subject that should be explored.

Acknowledgements

Conflict of interest

The authors declare no competing financial interests.

Author details

Akira Kouchi[1], Takashi Shimonishi[2], Tomoya Yamazaki[1], Masashi Tsuge[1], Naoki Nakatani[3], Kenji Furuya[4], Hiromasa Niinomi[5], Yasuhiro Oba[1], Tetsuya Hama[6], Hiroyasu Katsuno[1], Naoki Watanabe[1] and Yuki Kimura[1]*

1 Institute of Low Temperature Science, Hokkaido University, Sapporo, Japan

2 Center for Transdisciplinary Research, Niigata University, Niigata, Japan

3 Department of Chemistry, Graduate School of Science and Engineering, Tokyo Metropolitan University, Hachioji, Tokyo, Japan

4 National Astronomical Observatory of Japan, Mitaka, Tokyo, Japan

5 Institute of Multidisciplinary Research for Advanced Materials, Tohoku University, Sendai, Japan

6 Komaba Institute for Science, University of Tokyo, Tokyo, Japan

*Address all correspondence to: ykimura@lowtem.hokudai.ac.jp

IntechOpen

References

[1] Hazen RM, Sholl DS. Chiral selection on inorganic crystalline surfaces. Nature Materials. 2003;**2**:367-374. DOI: 10.1038/nmat879

[2] Weissbuch I, Lahav M. Crystalline architectures as templates of relevance to the origins of homochirality. Chemical Reviews. 2011;**111**:3236-3267. DOI: 10.1021/cr1002479

[3] Soai K, Asymmetric autocatalysis. Chiral symmetry breaking and the origins of homochirality of organic molecules. Proceedings of the Japan Academy Series B. 2019;**95**:89-110. DOI: 10.2183/pjab.95.009

[4] Hazen RM. Chiral crystal faces of common rock-forming minerals. In: Palyi G, Zucchi C, Caglioti L, editors. Progress in Biological Chirality. Elsevier: Oxford; 2004. pp. 137-151

[5] Kouchi A, Tsuge M, Hama T, Niinomi H, Nakatani N, Shimonishi T, et al. Formation of chiral CO polyhedral crystals on icy interstellar grains. Monthly Notices of the Royal Astronomical Society. 2021;**505**: 1530-1542. DOI: 10.1093/mnras/stab1173

[6] Kouchi A, Tsuge M, Hama T, Oba Y, Okuzumi S, Sirono S-I, et al. Transmission electron microscopy study of the morphology of ices composed of H_2O, CO_2, and CO on refractory grains. The Astrophysical Journal. 2021;**918**:45. DOI: 10.3847/1538-4357/ac0ae6

[7] Boogert ACA, Gerakines PA, Whittet DCB. Observations of the icy universe. Annual Review of Astronomy and Astrophysics. 2015;**53**:541-581. DOI: 10.1146/annurev-astro-082214-122348

[8] Mumma MJ, Charnley SB. The chemical composition of comets-emerging taxinomies and natal heritage. Annual Review of Astronomy and Astrophysics. 2011;**49**:471-524. DOI: 10.1146/annurev-astro-081309-130811

[9] Watanabe N, Kouchi A. Ice surface reactions: A key to chemical evolution in space. Progress in Surface Science. 2008;**83**:439-489. DOI: 10.1016/j.progsurf.2008.10.001

[10] Hagen W, Tielens AGGM, Greenberg JM. The infrared spectra of amorphous solid water and ice Ic between 10 and 140 K. Chemical Physics. 1981;**56**:367-379. DOI: 10.1016/0301-0104(81)80158-9

[11] Whittet DCB. Observation of molecular ices. In: Millar TJ, Williams DA, editors. Dust and Chemistry in Astronomy. Bristol and Philadelphia: Institute of Physics Publishing; 1993. pp. 9-35

[12] Kouchi A, Yamamoto T, Kozasa T, Kuroda T, Greenberg JM. Conditions for condensation and preservation of amorphous ice and crystallinity of astrophysical ices. Astronomy and Astrophysics. 1994;**290**:1009-1018

[13] He J, Toriello FE, Emitiaz SM, Henning T, Vidali G. Phase transition of interstellar CO ice. The Astrpohysical Journal Letters. 2021;**915**:L23. DOI: 10.3847/2041-8213/ac0a7c

[14] Luna R, Molpeceres G, Ortigoso J, Satorre MA, Domingo M, Maté B. Densities, infrared band strengths, and optical constants of solid methanol. Astronomy and Astrophysics. 2018;**617**: A116. DOI: 10.1051/0004-6361/201833463

[15] Zanchet A, Rodríguez-Lazcano Y, Gálvez Ó, Herrero VJ, Escribano R, Maté B. Optical constants of NH_3 and

NH$_3$:N$_2$ amorphous ices in the near-infrared and mid-infrared regions. The Astrophysical Journal. 2013;**777**:26. DOI: 10.1088/0004-637X/777/1/26

[16] Huston T, Hisatsune IC, Heicklen J. Low-temperature infrared studies of some acid-base reactions. Canadian Journal of Chemistry. 1983;**61**: 2077-2088. DOI: 10.1139/v83-361

[17] Bertie JE, Shehata MR. Ammonia dihydrate: Preparation, x-ray powder diffraction pattern and infrared spectrum of NH$_3$·2H$_2$O at 100 K. The Journal of Chemical Physics. 1984;**81**: 27-30. DOI: 10.1063/1.447381

[18] Mills RL, Olinger B, Cromer DT. Structures and phase diagram of N$_2$ and CO to 13 GPa by x-ray diffraction. The Journal of Chemical Physics. 1986;**84**: 2837-2845. DOI: 10.1063/1.450310

[19] Wang L, Sun C, Xu H, Zhang J, Zhao Y, Guo W, et al. Neutron diffraction study of crystal structure and temperature driven molecular reorientation in solid α-CO. AIP Advances. 2020;**10**:045301. DOI: 10.1063/1.5121337

[20] Vegard I. Struktur und Leuchtfähigkeit von festem Kohlenoxyd. Zeitschrift für Physik. 1930;**61**:185-190. DOI: 10.1007/BF01339658

[21] Petrenko VF, Whitworth RW. Physics of Ice. New York: Oxford University Press; 1999. p. 373. DOI: 10.1093/acprof:oso/9780198518945. 001.0001

[22] Tajima Y, Matsuo T, Suga H. Phase transition in KOH-doped hexagonal ice. Nature. 1982;**299**:810-812. DOI: 10.1038/ 299810a0

[23] Leadbetter AJ, Ward RC, Clark JW, Tucker PA, Matsuo T, Suga H. The equilibrium low-temperature structure of ice. The Journal of Chemical Physics. 1985;**82**:424-428. DOI: 10.1063/1.448763

[24] Kawada S. Dielectric dispersion and phase transition of KOH doped ice. Journal of the Physical Society of Japan. 1972;**32**:1442-1442. DOI: 10.1143/ JPSJ.32.1442

[25] Minagawa I. Phase transition of cubic ice Ic. Journal of the Physical Society of Japan. 1985;**54**:1610-1614. DOI: 10.1143/JPSJ.54.1610

[26] Lekner J. Electrostatics of proton arrangements in ice Ic. Physica B: Condensed Matter. 1997;**240**: 263-272. DOI: 10.1016/S0921-4526(97) 00430-4

[27] Casassa S, Calatayud M, Doll K, Minot C, Pisani C. Proton ordered cubic and hexagonal periodic models of ordinary ice. Chemical Physics Letters. 2005;**409**:110-117. DOI: 10.1016/ j.cplett.2005.04.068

[28] Raza Z, Alfè D, Salzmann CG, Klimeš J, Michaelides A, Slater B. Proton ordering in cubic ice and hexagonal ice; a potential new ice phase—XIc. Physical Chemistry Chemical Physics. 2011;**13**: 19788-19795. DOI: 10.1039/c1cp22506e

[29] Geiger P, Dellago C, Macher M, Franchini C, Kresse G, Bernard J, et al. Proton ordering of cubic ice Ic: Spectroscopy and computer simulations. Journal of Physical Chemistry C. 2014; **118**:10989-10997. DOI: 10.1021/ jp500324x

[30] Kouchi A, Yamazaki T, Katsuno H, Nada H, Hama T, Kimura Y. Possible formation of hydrogen-ordered cubic ice polymorphs by annealing of pure ice Ic at 100–130 K. Submitted to Journal Physical Chemistry

[31] Londono JD, Kuhs WF, Finney JL. Neutron diffraction studies of ices III and IX on under-pressure and recovered samples. The Journal of Chemical Physics. 1993;**98**:4878-4888. DOI: 10.1063/1.464942

[32] Cervinka C, Beran GJO. Ab initio prediction of the polymorph phase diagram for crystalline methanol. Chemical Science. 2018;**9**:4622-4629. DOI: 10.1039/c8sc01237g

[33] Torrie BH, Weng S-X, Powell BM. Structure of the α-phase of solid methanol. Molecular Physics. 1989;**67**:575-581. DOI: 10.1080/00268978900101291

[34] Furuya K, Hama T, Oba Y, Kouchi A, Watanabe N, Aikawa Y. Diffusion activation energy and desorption activation energy for astrochemicaly relevant species on water ice show no clear relation. The Astrophysical Journal Letters. 2022;**933**: L16. DOI: 10.3847/2041-8213/ac78e9

[35] Sugisaki M, Suga H, Seki S. Calorimetric study of the glassy state. III. Novel type calorimeter for study of glassy state and heat capacity of glassy methanol. Bulletin of the Chemical Society of Japan. 1968;**41**:2586-2591. DOI: 10.1246/bcsj.41.2586

[36] Ninet S, Dachi F. High pressure-high temperature phase diagram of ammonia. The Journal of Chemical Physics. 2008; **128**:154508. DOI: 10.1063/1.2903491

[37] Olovsson I, Templeton D. X-ray study of solid ammonia. Acta Crystallographica. 1959;**12**:832-836. DOI: 10.1107/S0365110X59002420

[38] Reed JW, Harris PM. Neutron diffraction study of solid deuteroammonia. The Journal of Chemical Physics. 1961;**35**:1730-1737. DOI: 10.1063/1.1732137

[39] Hewat AW, Riekel C. The crystal structure of deutroammonia between 2 and 180 K by neutron powder profile refinement. Acra Crystallographica. 1979;**A35**:569-571. DOI: 10.1107/S0567739479001340

[40] Dawes A, Mukerji RJ, Davis MP, Holtom PD, Webb SM, Sivaraman B. Morphological study into the temperature dependence of solid ammonia under astrochemical conditions using vacuum ultraviolet and Fourier-tansform infrared spectroscopy. The Journal of Chemical Physics. 2007; **126**:244711. DOI: 10.1063/1.2743426

[41] Fortes AD, Suard E, Lemée-Cailleau M-H, Pickard CJ, Needs RJ. Equation of state and phase transition of deuterated ammonia monohydrate ($ND_3·D_2O$) measured by high-resolution neutron powder diffraction up to 500 MPa. The Journal of Chemical Physics. 2009;**131**: 154503. DOI: 10.1063/1.3245858

[42] Loveday JS, Nelmes RJ. The ammonia hydrates—Model mixed-hydrogenbonded systems. High Pressure Research. 2004;**24**:45-55. DOI: 10.1080/08957950410001661990

[43] Fortes AD, Wood IG, Brodholt JP, Vočadlo L. The structure, ordering and equation of state of ammonia dehydrate (nh3·2h2o). Icarus. 2003;**162**:59-73. DOI: 10.1016/S0019-1035(02)00073-8

[44] Fortes AD, Wood IG, Brodholt JP. A high-resolution neutron powder diffraction study of ammonia dehydrate ($ND_3·2D_2O$) phase I. The Journal of Chemical Physics. 2003;**119**: 10806-10813. DOI: 10.1063/1.1619371

[45] Yamamoto T, Kataoka Y, Okada K. Theory of phase transitions in solid

methanes. X. Centering around phase II in solid CH$_4$. The Journal of Chemical Physics. 1977;**66**:2701-2730. DOI: 10.1063/1.434218

[46] Savoie R, Fournier RP. Far-infrared spectra of condensed methane and methane-*d*$_4$. Chemical Physics Letters. 1970;**7**:1-3. DOI: 10.1016/0009-2614(70)80232-9

[47] Hashimoto M, Hashimoto M, Isobe T. On the crystal structure of methane in phase II. Bulletin of the Chemical Society of Japan. 1971;**44**:2272-2274. DOI: 10.1246/bcsj.44.2272

[48] Press W. Structure and phase transitions of solid heavy methane (CD$_4$). The Journal of Chemical Physics. 1972;**56**:2597-2609. DOI: 10.1063/1.1677586

[49] Kobashi K, Okada K, Yamamoto T. Theory of phase transitions in solid methanes. XI. Infrared and Raman spectra of the ν_3 and ν_4 modes in phase II of solid CH$_4$. The Journal of Chemical Physics. 1977;**66**:5568-5577. DOI: 10.1063/1.433879

[50] Grieger S, Friedrich H, Guckelsberger K, Scherm R, Press W. The total neutron scattering cross section of solid methane in phase II. The Journal of Chemical Physics. 1998;**109**:3161-3175. DOI: 10.1063/1.476907

[51] Bonner WA. The origin and amplification of biomolecular chirality. Origin of Life and Evolution of the Biosphere. 1991;**21**:59-111. DOI: 10.1007/BF01809580

[52] Bailey J. Astronomical sources of circularly polarized light and the origin of homochirality. Origin of Life and Evolution of the Biosphere. 2001;**31**:167-183. DOI: 10.1023/A:1006751425919

[53] Greenberg JM, Kouchi A, Niessen W, Irth H, van Paradijs J, de Groot MS, et al. Interstellar dust, chirality, comets and the origins of life: Life from dead stars? Journal of Biological Physics. 1995;**20**:61-70. DOI: 10.1007/BF00700421

[54] Bailey J, Chrysostomou A, Hough JH, Gledhill TM, McCall A, Clark S, et al. Circular polarization in star-formation regions: Implications for biomolecular homochirality. Science. 1998;**281**:672-674. DOI: 10.1126/science.281.5377.672

[55] Weingartner JC, Draine BT. Dust grain-size distributions and extinction in the milky way, large Magellanic cloud, and small Magellanic cloud. The Astrophysical Journal. 2001;**548**:296-309. DOI: 10.1086/318651

[56] Whittet DCB, Gerakines PA, Hough JH, Shenoy SS. Interstellar extinction and polarization in the Taurus dark clouds: The optical properties of dust near the diffuse/dense cloud interface. The Astrophysical Journal. 2001;**547**:872-884. DOI: 10.1086/318421

[57] Mathis JS, Mezger PG, Panagia N. Interstellar radiation field and dust temperatures in the diffuse interstellar medium and in giant molecular clouds. Astronomy and Astrophysics. 1983;**128**:212-229

[58] Fukue T, Tamura M, Kandori R, Kusakabe N, Hough JH, Baily J, et al. Extended high circular polarization in the Orion massive star forming region: Implications for the origin of homochirality in the solar system. Origin of Life and Evolution of the Biosphere. 2010;**40**:335-346. DOI: 10.1007/s11084-010-9206-1

[59] Kwon J, Tamura M, Hough JH, Kusakabe N, Nagata T, Nakajima Y, et al.

Near-infrared circular polarization survey in star-forming regions: Correlations and trends. The Astrophysical Journal Letters. 2014;**795**: L16. DOI: 10.1088/2041-8205/795/L16

[60] Martin PG. Interstellar polarization from a medium with changing grain alignment. The Astrophysical Journal. 1974;**187**:461-472. DOI: 10.1086/152655

[61] Lucas PW, Hough JH, Bailey J, Chrysostomou A, Gledhill TM, McCall A. UV circular polarization in star formation regions: The origin of homochirality? Origin of Life and Evolution of the Biosphere. 2005;**35**: 29-60. DOI: 10.1007/s11084-005-7770-6

[62] Prasad SS, Tarafdar SP. UV radiation field inside dense clouds - its possible existence and chemical implications. The Astrophysical Journal. 1983;**267**: 603-609. DOI: 10.1086/160896

[63] Gredel R, Lepp S, Dalgarno A, Herbst E. Cosmic-ray–induced photodissociation and photoionization rates of interstellar molecules. The Astrophysical Journal. 1989;**347**:289-293. DOI: 10.1086/168117

[64] Shen CJ, Greenberg JM, Schutte WA, van Dishoeck EF. Cosmic ray induced explosive chemical desorption in dense clouds. Astronomy and Astrophysics. 2004;**415**:203-215. DOI: 10.1051/0004-6361:20031669

[65] Zhang H, Govorov AO. Giant circular dichroism of a molecule in a region of strong plasmon resonances between two neighboring gold nanocrystals. Physical Review B. 2013; **87**:075410. DOI: 1098-0121/2013/87(7)/ 075410(8)

[66] Wang R-Y, Wang P, Liu Y, Zhao W, Zhai D, Hong X, et al. Experimental observation of giant chiroptical

amplification of small chiral molecules by gold nanosphere clusters. Journal of Physical Chemistry C. 2014;**118**: 9690-9695. DOI: 10.1021/jp5025813

[67] Vestler D, Ben-Moshe A, Markovich G. Enhancement of circular dichroism of a chiral material by dielectric nanospheres. Journal of Physical Chemistry C. 2019;**123**: 5017-5022. DOI: 10.1021/acs. jpcc.8b10975

[68] Niinomi H, Sugiyama T, Tagawa M, Murayama K, Harada S, Ujihara T. Enantioselective amplification on circularly polarized laser-induced chiral nucleation from a $NaClO_3$ solution containing Ag nanoparticles. CrystEngComm. 2016;**18**:7441-7448. DOI: 10.1039/c6ce01464j

[69] Cheng AC, Niinomi H, Omatsu T, Ishida S, Sasaki K, Sugiyama T. Plasmonic manipulation-controlled chiral crystallization of sodium chlorate. Journal of Physical Chemistry Letters. 2020;**11**:4422-4426. DOI: 10.1021/acs. jpclett.0c01041

[70] Tang Y, Cohen AE. Optical chirality and its interaction with matter. Physical Review Letters. 2010;**104**:163901. DOI: 10.1103/PhysRevLett.104.163901

[71] Liu Y, Zhao W, Ji Y, Wang R-Y, Wu X, Zhang XD. Strong superchiral field in hot spots and its interaction with chiral molecules. Europhysics Letters. 2015;**110**:17008. DOI: 10.1209/ 0295-5075/110/17008

[72] Ho C-S, García-Extarri A, Zhao Y, Dionne J. Enhancing enantioselective absorption using dielectric nanospheres. ACS Photonics. 2016;**4**:197-203. DOI: 10.1021/acsphotonics.6b00701

[73] Ciesla FJ, Sandford SA. Organic synthesis via irradiation and warming of

ice grains in the solar nebula. Science. 2012;**336**:452-454. DOI: 10.1126/science.1217291

[74] Cuppen HM, Walsh C, Lamberts T, Semenov D, Garrod RT, Penteado EM, et al. Grain surface models and data for astrochemistry. Space Science Reviews. 2017;**212**:1-58. DOI: 10.1007/s11214-016-0319-3